



Microstructure, Mechanical, Tribological and Synergistic strengthening mechanisms of nickel/graphene nanoplatelets hybrid reinforced AZ91D magnesium-based matrix composites via spark plasma sintering

Olugbenga Ogunbiyi^{a,*}, Samuel A. Iwarere^{a,**}, Rotimi Sadiku^b, Michael O. Daramola^a

^a Department of Chemical Engineering, Faculty of Engineering, Built Environment and Information Technology, University of Pretoria, Hatfield, 0028, Pretoria, South Africa

^b Department of Chemical, Metallurgical and Materials Engineering, Tshwane University of Technology, Pretoria, 0001, South Africa

ARTICLE INFO

Handling editor: SN Monteiro

Keywords:

AZ91D-Ni-GNPs composite
Spark plasma sintering
Strengthening mechanism

ABSTRACT

AZ91D-Ni-graphene nanoplatelets (GNPs) Mg-based composites were effectively consolidated using spark plasma sintering (SPS). The - reinforcement in the AZ91D Mg alloy varies from 0 wt% to 2 wt%, with Ni constituent fixed at 1.5 wt%. Scanning electron microscope, Transmission electron microscope, X-ray diffraction and Raman spectroscopy were utilised to investigate the morphology of the powder and sintered compact. The synergistic strengthening offered by the inclusion of GNPs comprising grain refinement ($\Delta\sigma_{Hall-Petch}$), load transfer from AZ91D-Ni Mg-based alloy matrix to GNPs reinforcement ($\Delta\sigma_{LT}$), dislocations strengthening due to the mismatch in the coefficient of thermal expansion (CTE) ($\Delta\sigma_{CTE}$), modulus mismatch ($\Delta\sigma_{mm}$), and strengthening due to Orowan ($\Delta\sigma_{Orowan}$) was investigated. Experimental results indicate that the addition of GNPs contributes minimally to the densification of the compacts, increasing from 97% to 98.1% with increasing GNPs. However, significant improvements were obtained for other properties investigated, such as a microhardness, which increased from 67.4 to 89.7 H V, nano hardness from 4744.9 to 18,251.3 MPa, an elastic modulus from 84.53 to 243.75 GPa and wear rate from 5.21×10^{-3} to 3.85×10^{-3} mm³/N/m under 10 N load with an increase in GNPs content. This study establishes the capability of GNPs as efficient reinforcement in manufacturing metal matrix composites with enhanced mechanical and tribological properties.

1. Introduction

The demand for lightweight multifunctional structural materials has increased considerably over the past decades because of the advantages they offer in different applications [1]. For example, lightweight materials improve fuel efficiency and reduce emissions in the automobile industry (vehicles). Similarly, they improve components' strength in the electronic and aerospace industries [2]. Mg is primarily considered in applications that require high weight-saving because of its low density of 1.74 g/cm³, which is approximately 80%, 75%, 33%, and 60% lighter than Ni, steel, Al and Ti, respectively, thus becoming the lightest identified structural material [3]. The application of Mg alloys also extends to the biomedical field because Mg has comparable mechanical properties with human bone [4] and other excellent properties such as high specific strengths, exceptional damping properties, good machinability,

high stiffness, low densities and outstanding castability [5]. Despite the numerous advantages of Mg alloys, their applications are somewhat limited in some industrial fields because of their drawbacks, such as poor thermal stability, low wear resistance, low ductility, high oxidation rate, low strength, and hardness [4,6,7].

Hence, numerous reinforcement materials have been applied to Mg alloy matrices to develop excellent Mg-matrix composites, such as SiC, Al₂O₃, Ni, Al, CNTs, and GNPs, with a view to address some of the challenges identified [1]. In particular, Hassan et al. [8] investigated the influence of Ni reinforcement in Mg using varied fractions of Ni. It was established that 1.5% Ni contributes to forming strong interfacial bonding without resulting in any reaction (defects) in the final product (Ni-Mg alloy). Significant grain refinement was achieved with minimal porosity and high mechanical properties. To ensure that reinforcements significantly improve the strength of the Mg matrix in composite

* Corresponding author.

** Corresponding author.

E-mail addresses: olugbengaogunbiyi@gmail.com (O. Ogunbiyi), samuel.iwarere@up.ac.za (S.A. Iwarere).

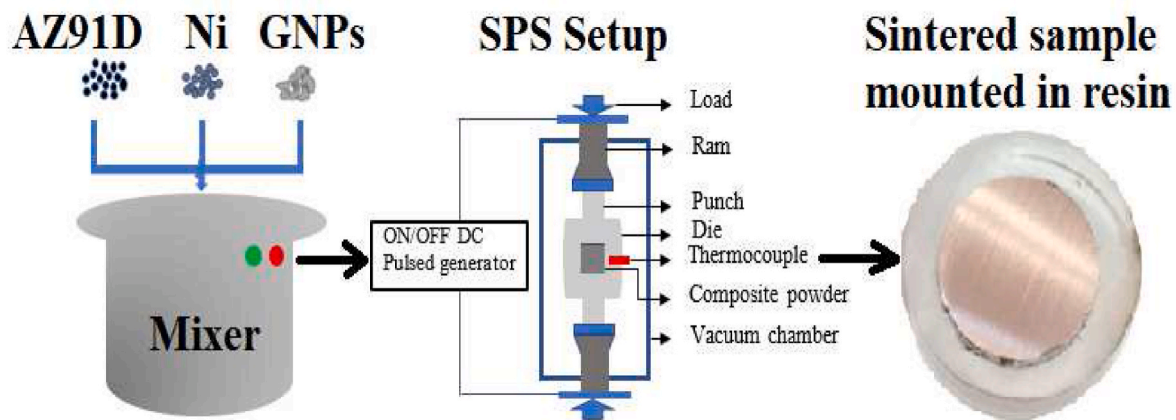


Fig. 1. Schematic illustration of the manufacturing process of Mg-based AZ91D-Ni alloy and AZ91D-Ni-GNPs composites.

materials and to tailor the properties of Mg-based composites in addressing specific applications, parameters such as the type of reinforcement, quantity, size, and processing methods are carefully considered. Amongst the metals that have been used as reinforcements to form part of Mg composites, Ni particles have displayed considerable potential in improving the strength of Mg alloys manufactured through powder metallurgy and ingot processing techniques [8,9]. On the other hand, carbonaceous and ceramic reinforcement have attracted significant attention in materials development research because of their outstanding mechanical, thermal, tribology, electrical and optical properties [10,11]. Multi-layer graphene, such as graphene nanoplatelets (GNPs), is a two-dimensional carbon nanomaterial that displays many outstanding properties of single-layer graphene, and this portrays them as a suitable reinforcing filler for metal alloys, especially Mg-alloys matrices [12–15]. However, to ensure load transfer between GNP reinforcement and the Mg matrix, it must be ensured that the GNPs are well dispersed in the Mg matrix because the composite's performance depends on the homogeneity of the mixture.

While different studies have shown the beneficial potential of GNPs as reinforcement in different metal alloy matrices, particularly with Mg alloys [16,17], the improvements in matrices could not only be attributed to the effect of the reinforcements alone but also to the manufacturing techniques. Spark plasma sintering (SPS) is a powder metallurgy (PM) technique that offers several benefits compared to traditional sintering processes [18]. It offers fast manufacturing at high sintering temperatures and rapid heating rates that result in the realisation of uniform microstructure in the fabricated components. SPS operating procedure and advantages have been widely reported in the literature, including the influence of its process parameters [19]. Consequently, a suitable combination of reinforcements and processing techniques will help to improve the physical, microstructural, mechanical and tribological properties of Mg matrix alloys. Therefore, considering the existing gaps, the primary contributions of this paper center around threefold. Firstly, the improvement of AZ91D Mg alloy through micro and nano reinforcement using spark plasma sintering technology. Secondly, to provide a material that is comparably competitive in terms of strength and properties and to make a case for its adoption. Thirdly, to establish the strengthening mechanisms that contribute to the improvement of AZ91D Mg matrix alloy using micro and nano reinforcement. To put things in perspective, the present work investigates the microstructure, mechanical, tribology, and synergistic strengthening mechanisms of Ni and GNPs hybrid reinforced AZ91D Mg-based matrix composites via SPS technique.

2. Experimental details

The experimental and characterisation processes are explained

briefly, with full detail explained in the supplementary information (S1). The starting materials are in powder form and were thoroughly mixed using effective powder mixing procedures to obtain homogenous admixed powders. Subsequently, the admixed powder was transferred to the SPS machine for consolidation. Thereafter, the developed composites' microstructure mechanical and tribological properties were tested. The gas-atomised AZ91D Mg-based alloy (matrix starting powder) with 99.7% purity and spherical particle size ranges between 15 and 53 μm was obtained from Dome metal in China. Wear Tech Ltd, South Africa, supplied the Ni powder with 99.5% purity and spherical particle sizes between 0.5 and 3 μm , while GNPs were obtained from Sigma-Aldrich, South Africa. The GNPs has a surface area between 15 and 30 m^2/g , an average diameter of 5 μm and an average thickness of 15 nm, as obtained from the manufacturer. The percentage of Ni constituent is fixed at 1.5 wt% [8,9], while the GNP constituent varies from 0 to 2 wt% with reference to the AZ91D Mg alloy matrix. The blending and mixing were done in a tubular mixer and planetary ball milling (PM 400) in a dry and wet environment, using W balls to aid homogeneity. Subsequently, the admixed powder placed in the graphite die is transferred into the heating chamber of the SPS system (Model HHPD-23, FCT Germany) for sintering and consolidation processes. A pressure of 50 MPa, a heating rate of 100 $^\circ\text{C}/\text{min}$, a holding time of 5 min and a sintering temperature of 500 $^\circ\text{C}$ was used to produce a set of test samples. The schematic illustration of the manufacturing processes of AZ91D-Ni alloy and AZ91D-Ni-GNPs Mg-based composites is presented in Fig. 1.

The samples were metallographically prepared for further characterisation at the completion of the manufacturing process. The bulk relative density of the sintered AZ91D-Ni alloy and AZ91D-Ni-GNPs composites was measured following the Archimedes principle and according to the ASTM C373-88 standard [19]. The morphology of the as-received powders (AZ91D Mg alloy, Ni, GNPs), sintered alloy/composites (microstructure and elemental dispersion) and worn surfaces were observed using an optical microscope (Falcon 500 series), Zeiss Ultra Plus 55 field emission scanning electron microscope (FE-SEM), incorporated with energy dispersive X-ray (EDS) spectra operated at 1.0 kV and JEOL-2100F high-resolution transmission electron microscope (HRTEM FEI Tecnai-F30) operated at 200 kV accelerating voltage. The various phases formed in the sintered composites were identified using a PANalytical Empyrean X-ray diffractometry (XRD) at a scanning rate of 0.02 $^\circ/\text{sec}$ with $\text{CuK}\alpha$ radiation ($\lambda = 0.154 \text{ nm}$) at 50 kV and 30 mA over the angular range of 10–90 $^\circ$. A T64000 micro-Raman spectrometer (HORIBA Scientific, Jobin Yvon Technology) is used to characterise the sintered components operating at 514 nm laser wavelength and 120s spectral acquisition time following ASTM E1840-96 standard [20]. The optical micrographs displaying different grain shapes, sizes, and boundaries were characterised by assessing the area of the grains in each direction to quantify the grain size

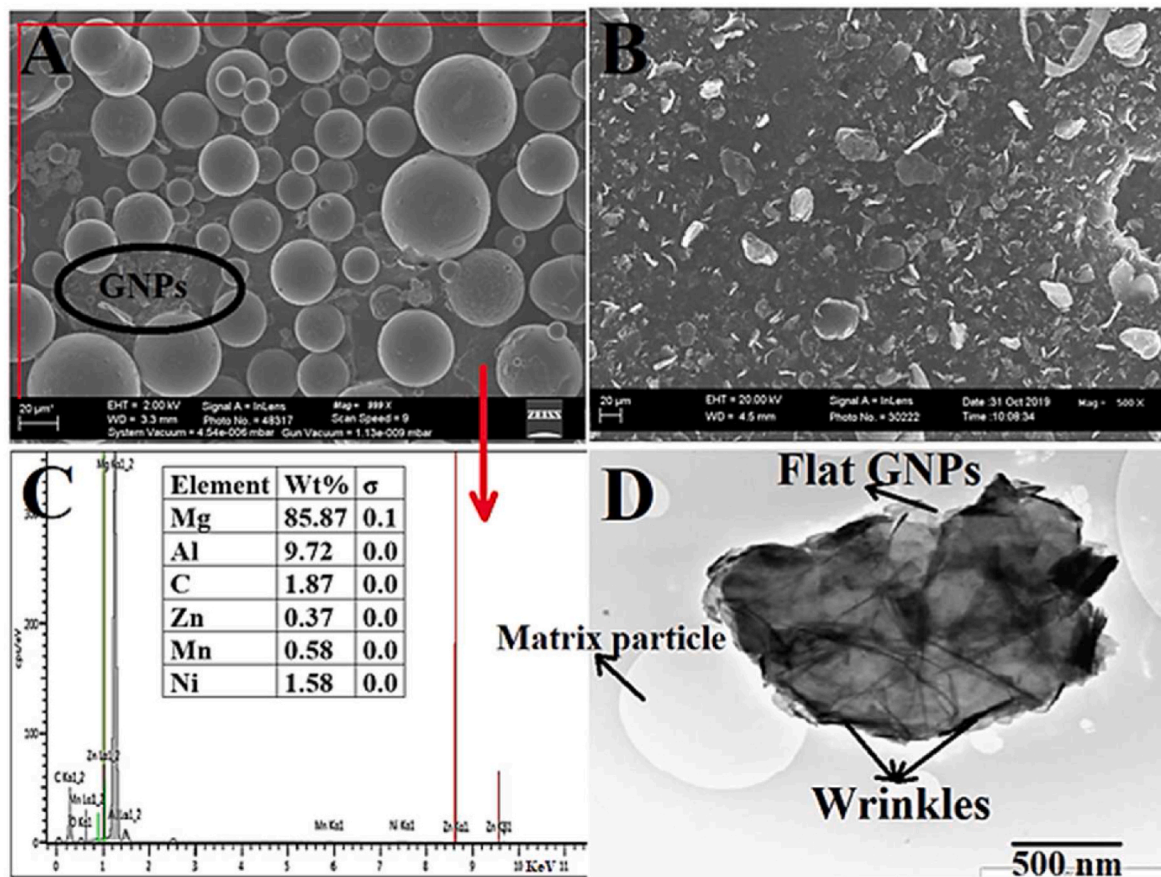


Fig. 2. Microstructure of the admixed composite powder and as-received GNP powder: (a) SEM image of the powder mixture (2 wt%), (b) SEM image of the as-received GNPs powder, (c) EDS image of the powder mixture, and (d) TEM image of the powder mixture (2 wt%).

distribution. An ImageJ graphics software is employed in this regard. The microhardness value of each material is evaluated using an automated digital Vickers microhardness tester (Future-tech). A load of 500 gf (5 N) and a dwell time of 15s were used for the polished test samples. The nanoindentation testing was conducted following the E2546-15 standard using Anton Paar (TTX-NHT) tester [21,22]. The dry sliding wear performance of the sintered AZ91D-Ni alloy and AZ91D-Ni-GNPs composites were examined at room temperature (RT ~ 24°C) utilising a tribometer (Anton Paar, TRB³) machine in accordance with ASTM G99-95 standard [23]. The wear testing is conducted using a pin-on-disc dry-sliding rotating part equipped with a wear and friction monitoring system operated at 300 rpm with a load of 10 N for 15 min (See

supplementary information for extensive experimental procedure).

3. Results and discussion

3.1. Microstructure analysis of the admixed and GNPs powder, sintered Mg-based AZ91D-Ni alloy and AZ91D-Ni-GNPs composite

The microstructures of the powder mixture and as-received GNPs powder with the corresponding EDS spectra of the powder mixture are shown in Fig. 2. As shown in Fig. 2a, b and 2d of the powder mixture, the SEM images revealed that the AZ91D Mg alloy matrix particles are spherical, Ni is irregular, and GNPs particle displays an irregular flake-

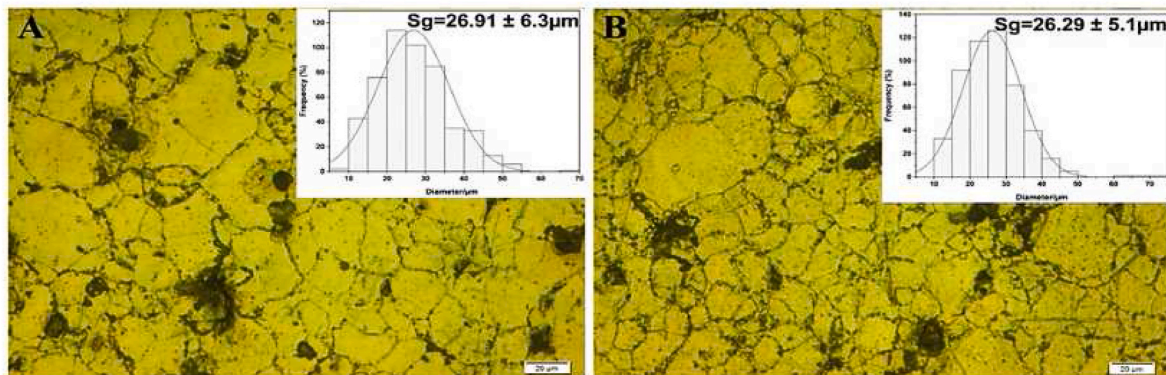


Fig. 3. Optical microstructures and grain size distribution of sintered Mg-based AZ91D-Ni alloy and AZ91D-Ni-GNPs composite (a) 0 wt% GNPs and (b) 0.5 wt% GNPs.

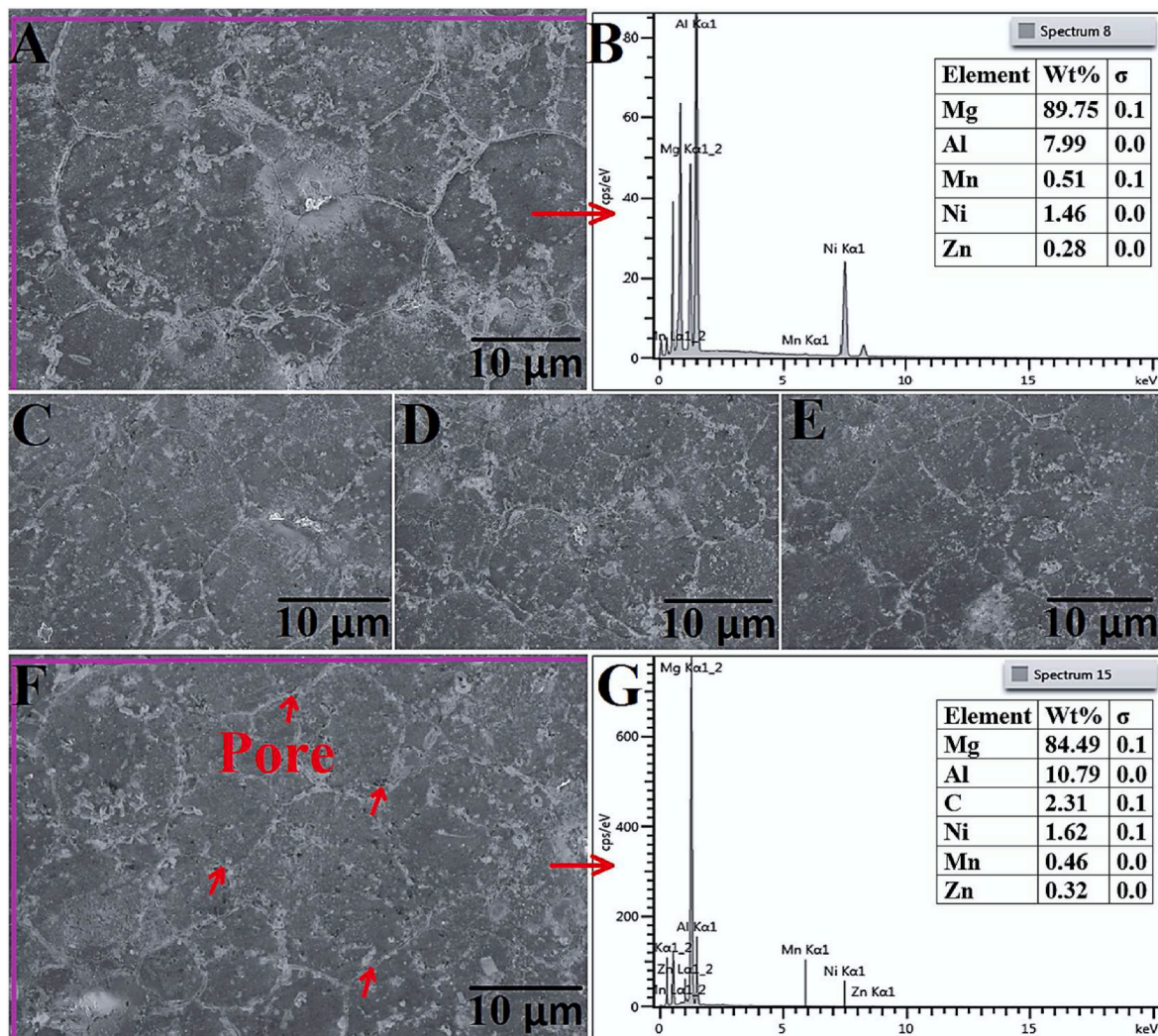


Fig. 4. SEM images of the sintered Mg-based AZ91D-Ni alloy and AZ91D-Ni-GNPs composites. (a) 0 wt% GNPs, (c) 0.5 wt% GNPs, (d) 1 wt% GNPs, (e) 1.5 wt% GNPs, (f) 2 wt% GNPs while (b) and (g) correspond to the EDS of (a) and (f) microstructures.

like morphology. The TEM image in Fig. 2d revealed the characteristics of an individual GNP in the matrix powder, and it shows that the GNP particle is flaky with both flat and wrinkled edges. The surface area analysis by EDS in Fig. 2c for the composite powder revealed the elemental composition present in the admixed composite powder. The peaks associated with Al, Zn and Mn elements were observed, proving the presence and dispersion of these elements in the Mg matrix. These elements are characteristics of AZ91D grade Mg alloy [24], which help improve the strength of the alloy and the formation of β -Mg₁₇Al₁₂ strengthening phase [25].

3.2. Microstructure analysis of the sintered Mg-based AZ91D-Ni alloy and AZ91D-Ni-GNPs composites

The Mg-based AZ91D-Ni alloy and GNP-reinforced AZ91D-Ni composites were effectively manufactured by alloying and spark plasma sintering powder metallurgy technique. Fig. 3a and b shows the optical microstructures of the sintered AZ91D-Ni alloy and GNPs reinforced Mg alloy with GNPs constituents of 0.5 wt%. The micrographs for the composite sintered with varied GNPs from 1 to 2 wt% (Fig. 3S c-e) are in the supplementary information. The optical micrographs reveal the presence of minimal defects such as surface micro-cracks and micropores, even with the increasing GNPs constituent, thus suggesting the formation of good metallurgical bonding between the grains. Although

the micrographs were obtained at low magnification, the result implied that there is good densification and metallurgical bonding between the matrix and reinforcement. Meanwhile, the grain boundaries are evident with the presence of small pores from the micrographs. The grains formed are in different shapes and sizes and were measured repeatedly in different directions (~ five hundred values) to establish the extent of microstructural refinement owing to the addition of GNPs reinforcement. The 0.5 wt% addition of GNPs to AZ91D-Ni alloy slightly affected the matrix microstructure. The measured grain sizes are inserted into the corresponding micrograph in Fig. 3a and b and 3S c-e. The average grain size is slightly reduced from 26.91 to 26.29 μ m. Subsequent addition of GNPs minimally influenced grain refinement by causing grain size reduction from 26.29 (0.5 wt%) to 23.35 μ m (2 wt%). While there is a marginal reduction in the average grain sizes of the composites developed with an increase in GNPs constituent, the mechanical and wear properties are greatly influenced.

Since the SPS technique promotes rapid densification [26], the influence of GNPs on densification may be restricted [27]. This observation agrees with Minarik Y. et al. [28] study, where graphene sheets were utilised to reinforce ZK61 Mg alloy making use of SPS, which is similar to this study. It may be inferred that the heterogeneous formation of grain size is associated with the heterogeneous dispersion of GNPs because of an increase in GNP constituents. The development of grains in the sintered components is brought about by the

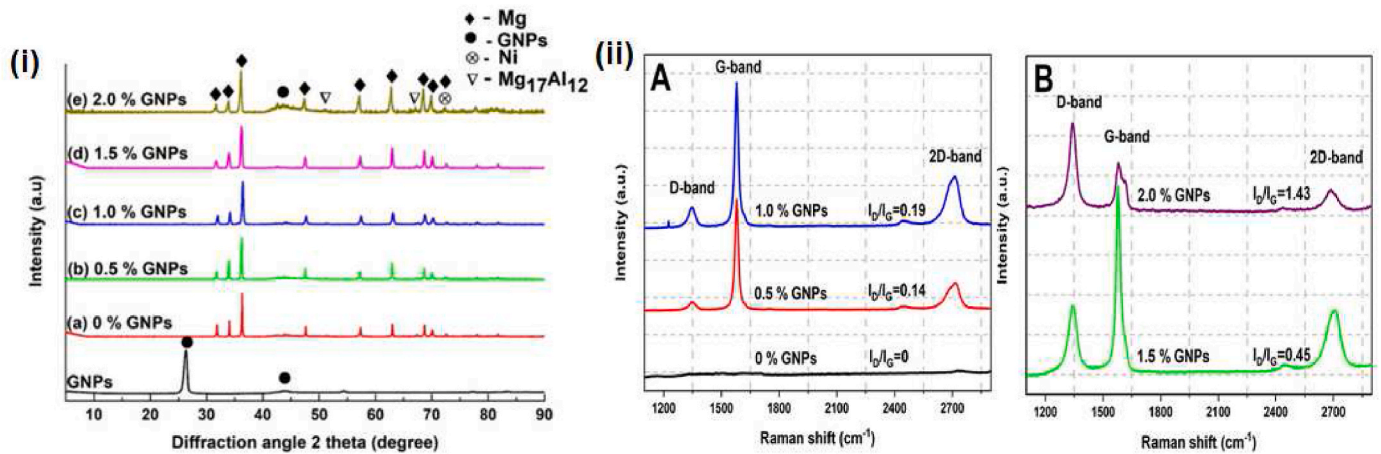


Fig. 5. (I) XRD patterns and (IIa and b) Raman spectra of GNPs powder, sintered Mg-based AZ91D-Ni alloy and AZ91D-Ni-GNPs composites.

recrystallisation of grains along the initial particle boundaries of AZ91D matrix powder [28] and recrystallisation owing to the reinforcement (Ni/GNPs) particles [8,29], which act as a catalyst for grain formation. The microstructures displayed two essential regions: the dominant light brown and minimal dark brown region, which were later investigated using SEM. The presence of minimal defects is attributed to the fact that the process parameters employed are adequate, leading to high densification and the formation of strong metallurgical bonding within the microstructure of the sintered components. In addition, the high standard deviation error is obtained from the diverse character, features and grain size dispersion [28].

Furthermore, the SEM and EDS analyses further explain the sintered components' microstructural features. Fig. 4a–c, d, e, and f show the SEM micrographs of the sintered Mg-based AZ91D-Ni alloy and AZ91D-Ni-GNPs composites, and in contrast, Fig. 4b and g shows the EDS analysis of Mg alloy (EDS of Fig. A) and 2 wt% GNPs reinforced AZ91D-Ni-GNPs composite (EDS of Fig. F). According to the SEM micrographs of the sintered AZ91D-Ni-GNPs composite, the microstructural features are assessed in terms of: (a) distribution of GNPs reinforcement (EDS) and (b) surface morphology. From the EDS results presented in Fig. 4b and g, Al is the second dominant element after Mg, suggesting the possible formation of α -Mg₁₇Al₁₂ strengthening phase [27], a phase later confirmed from the XRD analysis. The grain shapes are spherical and irregular, demonstrating that sintering ensued through grain recrystallisation, neck formation, and grain growth, leading to high densification of the sintered AZ91D-Ni-GNPs composites. The micropores are formed mainly at the contact points between the grains (along grain boundaries), and fewer micropores are formed within the grains. The high-magnification imaging inserted in Fig. 5 indicates the presence of porosity formation along the grain boundaries.

Considering the quantity of GNPs and Ni added to the AZ91D matrix confirmed by the percentages composition (revealed by the EDS), obtaining agglomerates or clusters within the microstructure [30] may be minimal. In addition, the shapes of the grains suggest that the initial particle shape is retained with a mixture of new grains after sintering, thus indicating heterogeneity in grain size formation and non-uniformity during grain refinement. This may result from the temperature distribution and uneven dispersion of GNPs [31,32]. With the small amount of GNPs and Ni reinforcement (~ 3 wt%), there may not be a recognisable presence of periodic high-particle clustered regions along the grain boundaries and within the grains [27]. This suggests that a good metallurgical bonding exists between the reinforcements and AZ91D matrix alloy [27]. Other trace elements in the matrix alloy have minimal influence apart from Al, as shown in Fig. 4b and f EDS analysis.

3.3. XRD and Raman spectroscopy analyses of GNPs, sintered Mg-based AZ91D-Ni alloy and AZ91D-Ni-GNPs composites

The XRD spectra of GNPs powder, sintered mg-based AZ91D-Ni alloy and AZ91D-Ni-GNPs composites with different fractions of GNPs denoted as samples A - E are shown in Fig. 5I. It is apparent that the peaks detected in the sintered Mg-based composites represent the presence of Mg, Ni, C (GNPs) and Mg₁₇Al₁₂. C is carbon, which has the same characteristics as GNPs. Only one peak representing the presence of C (002) is observed in the sintered composite with 2 wt% GNPs reinforcement, while there are no conspicuous peaks representing C in the composites sintered with < 2 wt% GNPs. The intensity of the peak representing GNPs increases with increasing GNPs content compared with the sample with < 2 wt% GNPs content; thus, the obvious peak representing GNPs observed in sample E (2 wt% GNPs) at an angle of 44°. The other peaks representing the Mg matrix, Ni and Mg₁₇Al₁₂ are evident at different 2θ angles of diffraction: 32.2°, 34.3°, 36.7°, 47.6°, 57.4°, 63.2°, 68.5°, 70.0 and 72.8° for Mg matrix, 72.8° for Ni, and 51.4° and 66.3° for Mg₁₇Al₁₂. Parizi et al. [33] could not detect the presence of GNPs in their study on the influence of varied GNPs contents on the mechanical properties and microstructure of AZ80 Mg alloy. This was due to a smaller fraction of GNPs reinforcement used (≤ 0.6 wt%, GNPs); thus, XRD spectra could not detect the presence of GNPs. However, the increasing amount of GNPs reinforcement in AZ91D-Ni alloy up to 2 wt% reveals a peak representing the presence of GNPs. Similarly, peaks representing Mg and Mg₁₇Al₁₂ phases were obvious in their study at the same diffraction angle as obtained in this study, thus confirming the observation. Furthermore, the intensity of the peak representing the strengthening Mg₁₇Al₁₂ phase is small owing to the smaller amount of Al constituent present in the AZ91D alloy [34]. The limited information obtained in the composites resulting from GNPs reinforcement necessitates further investigation using Raman spectroscopy analysis.

Characterising the structural transformations in sp² carbonaceous GNPs reinforcement with respect to the processing conditions and synergistic effect with neighbouring metal matrices is important in evaluating its reinforcing effectiveness in the developed composite. The chemical stability of GNPs reinforcement, phase transformations, and bonding effectiveness with neighbouring AZ91D-Ni matrices play a part in strengthening Mg matrix alloys. Thus, Fig. 5(II) shows the Raman spectra of the sintered composites with varying weight percentages of GNPs constituents. Noteworthy is that Mg, the dominant metal in the sintered components with other metals present in a smaller amount, exhibits similar Raman characteristics to most other metals, i.e. they do not show evidence of Raman active vibrational modes. On the other hand, the Raman spectra for the GNPs reinforcement present in the composites revealed three prominent peaks at 1345, 1579 and 1688

Table 1

Raman data from the spectra obtained for the sintered Mg-based AZ91D-Ni alloy and AZ91D-Ni-GNPs composites and variations in I_D/I_G , I_{2D}/I_G and I_G/I_{2D} intensity ratios.

Samples (varied GNPs constituent)		Peak Information (y (a.u.) and x (cm^{-1}) axis)							
Material grade	GNPs	D-band	G-band	2D-band	I_D/I_G	I_{2D}/I_G	I_G/I_{2D}		
AZ91D-Ni-GNPs Mg-based composites grade	0	–	–	–	–	–	–	–	
	0.5	y-2,158, x-1345	y-15,950, x-1579	y-4,738, x-2688	0.14 ± 0.02	0.30 ± 0.03	3.36 ± 0.06		
	1.0	y-4,000, x-1345	y-20,709, x-1579	y-8,134, x-2888	0.19 ± 0.03	0.39 ± 0.05	2.54 ± 0.03		
	1.5	y-4,906, x-1345	y-10,922, x-1579	y-4,685, x-2688	0.45 ± 0.02	0.43 ± 0.02	2.33 ± 0.05		
	2.0	y-6,392, x-1345	y-4,407, x-1579	y-3,041, x-2688	1.43 ± 0.05	0.69 ± 0.06	1.44 ± 0.04		

cm^{-1} , which are characteristic of the D band, G band and 2D band, respectively [12]. The three bands are commonly related with first-order (G band) and second-order (double resonance D and 2D Bands) Raman scattering in GNPs [35]. Table 1 reports the information about the three prominent peaks obtained from the Raman analysis and ratios of the I_D/I_G , I_{2D}/I_G and I_G/I_{2D} for varied GNPs reinforced AZ91D-Ni-GNPs Mg-based composite grade.

The variations in the distinctive Raman peak intensity ratio I_D/I_G represent the inherent or induced disorders, and it is indicative of the degree of graphitisation and structural integrity of dispersed GNPs carbonaceous reinforcement in metal matrices [4]. Therefore, the smaller I_D/I_G ratio values were obtained in 0.5–1.5 wt% GNPs reinforced Mg-based composites, indicating a better degree of graphitisation and formation of reduced damage compared to 2 wt% GNPs reinforced composite (Table 1) [36]. The composite with 2 wt% GNPs has a 1.43 ratio of I_D/I_G , indicating that the damage present in GNPs is slightly high due to the slightly high volume fraction of GNPs and the effect of the ball added to the powder during preparation; thus, the reason for using a low mixing speed. The balls were added to aid in homogenous mixing. The peak intensity ratio of the I_G/I_{2D} band symbolises the number of layers existing in the GNPs reinforcement. A study reported by Guerra et al. [37] using a Raman spectroscopy method confirmed that GNPs possess several layers. It is confirmed from the result of the analysis that the intensity ratio I_G/I_{2D} could be utilised to identify single-layer GNPs, few-layers GNPs and multiple-layers GNPs. Thus, the quantitative indicators reported imply that the ratios of I_G/I_{2D} from 0.3 to 0.5, 0.5–1 and >1 correspond to the formation of single-layer, few-layers, and multiple-layers GNPs sheets.

The I_G/I_{2D} ratio of GNPs measured for the composites in this study are 0 , 3.36 ± 0.06 , 2.54 ± 0.03 , 2.33 ± 0.05 , and 1.44 ± 0.04 for 0–2 wt % GNPs reinforcement, respectively, suggesting that multiple layers of GNPs sheet were formed in all the components. Their corresponding I_D/I_G ratio, which signifies the degree of the disorder to graphitisation, were quantified as 0 , 0.14 ± 0.02 , 0.19 ± 0.03 , 0.45 ± 0.02 , and 1.43 ± 0.05 , respectively, for components reinforced with 0–2 wt% GNPs. It was observed that the Raman spectra (Fig. 5(II)a and b) of the sintered AZ91D-Ni-GNPs Mg-based composites containing varied GNPs showed somewhat broadened G bands at 1597 cm^{-1} with an increase in GNPs constituent. Munir et al. [38] indicated that this observation implies the presence of minor defects in the sp^2 C–C network of GNPs. Meanwhile, the ratio of I_{2D}/I_G of GNPs reinforcement increases with the increasing quantity of GNPs, suggesting the formation of strong interaction and bonding between individual GNPs [12]. Summarily, the strengthening mechanisms in composites comprising carbonaceous reinforcing materials such as GNPs precisely rely on the structural integrity of the reinforcements in the metal matrices. Also, strengthening mechanisms occur differently in metal matrix composites (MMCs) based on the characteristics and nature of defects buildup in the sp^2 carbon network in GNPs [4]. Thus, it becomes challenging to precisely predict the contribution of each strengthening mechanism to the strength of the MMCs, especially in Mg-based GNP-reinforced composites.

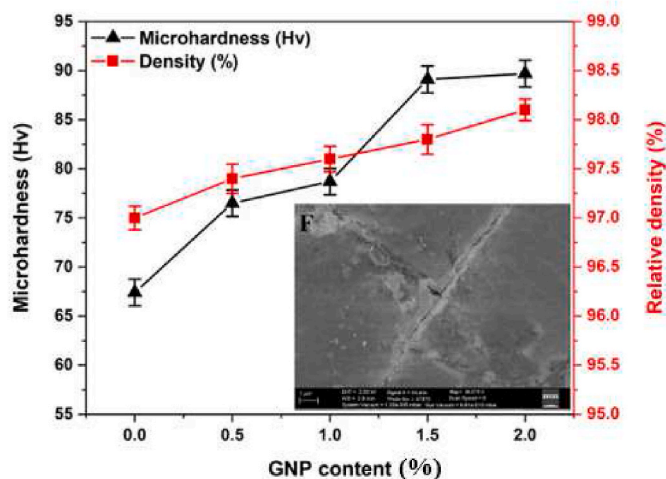


Fig. 6. Microhardness with the relative density of the sintered Mg-based AZ91D-Ni alloy and AZ91D-Ni-GNPs composites.

3.4. Mechanical and wear behaviour of the sintered Mg-based AZ91D-Ni alloy and AZ91D-Ni-GNPs composite

3.4.1. Microhardness and relative density measurements of the sintered Mg-based AZ91D-Ni alloy and AZ91D-Ni-GNPs composites

Fig. 6 shows the influences of fixed Ni and varied GNPs constituents on the microhardness and relative density of the developed Mg-based AZ91D-Ni alloy and AZ91D-Ni-GNPs composites. There is a slight difference of 1.1% margin between the composite sample with the highest GNPs content and the alloy without GNPs content. The sintered composite with 2 wt% GNPs content has 98.1% relative density, while the sample without GNPs has 97.0% relative density. The microhardness increases with the increasing GNPs constituent. Though the increasing constituent of GNPs in the matrix alloy increases the microhardness value of the sintered composite, a minimal difference in microhardness value is observed when comparing the sample with 1.5 wt% and 2 wt% GNPs constituents. The microhardness value of the alloy (sample without GNPs content) is 67.4 H V, and the microhardness value of the sample with the highest GNPs constituent (2 wt% GNPs) is 89.7 H V. This indicates that the microhardness value increased about 1.3 times. Between the alloy without GNPs and the composites with 0.5 wt% GNPs, the microhardness increased approximately 1.1 times. In general, the microhardness values are 67.4, 76.5, 78.7, 89.1 and 89.7 H V in the increasing order of GNPs constituents from 0 to 2 wt%. The increase in the microhardness property is associated with GNP and $\text{M}_{17}\text{Al}_{12}$ strengthening reinforcement/phase that confines the local deformation of Mg–Ni matrix during the indentation [39].

Similarly, the presence of GNPs helps in grain refinement, and the high sintering temperature promotes good interfacial bonding between GNPs reinforcement and the AZ91D-Ni matrix. Also, limited micropores are observed in the sintered alloy/composites, and few micro-cracks are present along the grain boundaries. The micro-crack is shown at high

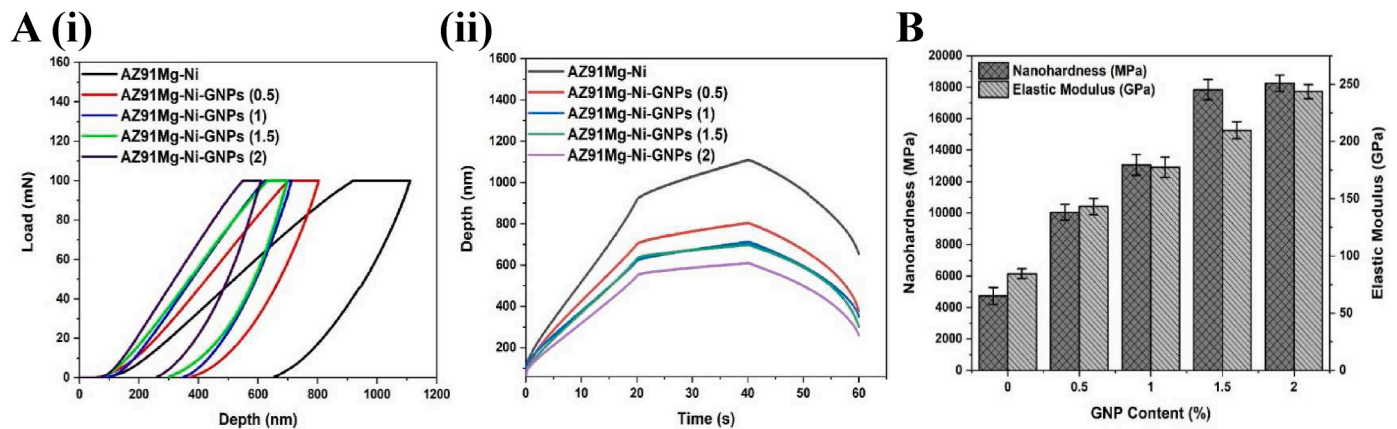


Fig. 7. Nanoindentation analysis of the sintered alloy and composites. (a) (I) and (II) Load-depth and Depth-time curves and (b) Nanoindentation hardness versus elastic modulus obtained from the nanoindentation of the sintered Mg-based AZ91D-Ni alloy and AZ91D-Ni-GNPs composites under an indentation load of 100 mN.

magnification in the micrograph of the sample with 2 wt% GNPs content inserted in Fig. 6. The presence of micro-crack implies that the components have a slight defect; however, it is not sufficient to impact the hardness property of the sintered components, as corroborated by the values of the relative densities obtained. The slight difference in the microhardness values of the components with 1.5 wt% and 2 wt% GNPs reinforcement suggests that the GNPs constituent is nearing the point where further addition may contribute minimally to the matrix alloy. Sun X. et al. [40], indicated that there is a tendency for GNPs to agglomerate in the Mg matrix at a percentage reinforcement above 1.5 wt% due to the excessive presence of GNPs. They reported a decrease in the microhardness value of GNPs/Mg reinforced with 2 wt% GNPs compared to GNPs/Mg composite with 1.5 wt% GNPs reinforcement.

3.4.2. Load-depth and depth-time curves of the sintered Mg-based AZ91D-Ni alloy and AZ91D-Ni-GNPs composites

The nanoindentation load-depth and depth-time curves of the sintered Mg-based AZ91D-Ni alloy and AZ91D-Ni-GNPs composites comprising 0, 0.5, 1.0, 1.5 and 2 wt% of GNPs after being subjected to indentation loads of 100 mN are demonstrated in Fig. 7a (I) and (II). From the curves developed after indentations, it is obvious that the alloy and composites, i.e., materials with and without GNPs, display comparable loading and unloading behaviours. The load-depth curves represent the elastic-plastic deformation performance of the sintered materials, and it is noticed that the unreinforced AZ91D-Ni alloy exhibited the highest penetration depth. The penetration depth reduced with an increase in the addition of GNPs in AZ91D-Ni-GNPs Mg-based composites grade, which suggests that the presence of GNPs helped improve the alloy. Subsequently, the improvement in strength and stiffness experienced with the sintered composites as a result of the GNPs reinforcement could emanate from the load transfer mechanism from matrix alloy to reinforcement GNPs. Correspondingly, similar observations were displayed in Fig. 7a (II), representing the penetration depth curves as a function of time for the sintered Mg-based AZ91D-Ni and AZ91D-Ni-GNPs composites comprising 0 to 2 wt% GNPs subjected to indentation load of 100 mN.

It is evident that both the sintered Mg alloy and composites experience immense plastic deformation. The maximum penetration depth is observed with the sample without GNPs, while the least penetration depth is obtained with the composite comprising 2 wt% GNPs corresponding to 1021.0454 and 609.9753 nm, respectively. Meanwhile, other sintered AZ91D-Ni-GNPs grades with 0.5, 1.0, and 1.5 wt% GNPs reinforcement have the highest penetration depth values of 800.8676, 712.1819 and 697.7902 nm, respectively. These results indicate that the AZ91D-Ni-GNPs grade possesses the highest hardness and stiffness properties resulting from the addition of GNPs. Thus, there is an appropriate load

transfer from the matrix to GNPs reinforcement; a strengthening mechanism offered by GNPs. The strengthening mechanism ensures the development of the pinning effect to resist dislocation motion through GNPs reinforcement in the AZ91D-Ni matrix [41]. Moreover, the sintered Mg-based AZ91D-Ni alloy and AZ91D-Ni-GNPs composites showed a similar time curve for the duration of the complete nano-indentation cycle. The plastic deformation is noticed even with the resistance to penetration demonstrated by the sintered materials (Fig. 7a), and there is a minimal disparity in the elastic-plastic behaviour between the sintered Mg-based AZ91D-Ni-GNPs composites in terms of depth-time curves. However, the depth-time curve for the sintered AZ91D-Ni alloy is minimally different, which may be attributed to the absence of GNPs reinforcement that should offer resistance to the dislocation motion during the nanoindentation test.

The nanoindentation hardness and elastic modulus of the sintered Mg-based AZ91D-Ni alloy and AZ91D-Ni-GNPs composites comprising a fixed 1.5 wt% Ni and varied 0, 0.5, 1, 1.5 and 2 wt% of GNPs, analysed with an indentation load of 100 mN, are displayed in Fig. 7b. From Fig. 7b, It was noticed that the nanoindentation hardness and modulus of elasticity values increased with the addition of GNPs reinforcement into the AZ91D matrix. Meanwhile, 2 wt% AZ91D-Ni-GNPs Mg-based composite illustrated the best nanoindentation hardness and modulus of elasticity values of 18,251.3 and 243.75 GPa, respectively. Also, the nanoindentation hardness and modulus of elasticity for adding 0, 0.5, 1.0 and 1.5 wt% of GNPs into AZ91D-Ni alloy are 4744.9, 10,049.2, 13,064.4, 17,837.6 MPa (nano-indentation hardness) and 84.53, 143.29, 177.54, 209.74 GPa (elastic modulus), respectively. The increasing nanoindentation hardness and modulus of elasticity values indicate that the sintered AZ91D-Ni-GNPs composites are tremendously enhanced with the addition of GNPs reinforcement. The high nanoindentation hardness value obtained with the sintered composite with 2 wt% GNPs implies that the grade has high resistance to plastic deformation: an observation confirmed in the load-depth curves in Fig. 7a. In addition, the enhancement in the strength of the sintered AZ91D-Ni-GNPs composites results from the hindrance to the movement of dislocation caused by the addition of GNPs reinforcement, which strengthens the AZ91D-Ni matrix. The GNPs reinforcement equally causes remarkable improvements in the modulus elasticity by ensuring that the composite grades elastically repel linear compression produced from the indenter. Conversely, the reduced grain size due to the microstructure refinement during sintering as a result of GNPs reinforcement contributes to the enhanced properties obtained in the sintered composite grade. According to the Hall-Petch relationship, reduced grain size increases the strength of materials. The presence of Al in the matrix alloy and the application of high sintering temperature aid diffusion and promote the formation of the $Mg_{17}Al_{12}$ strengthening phase that equally contributes to the improvement in the properties of the sintered

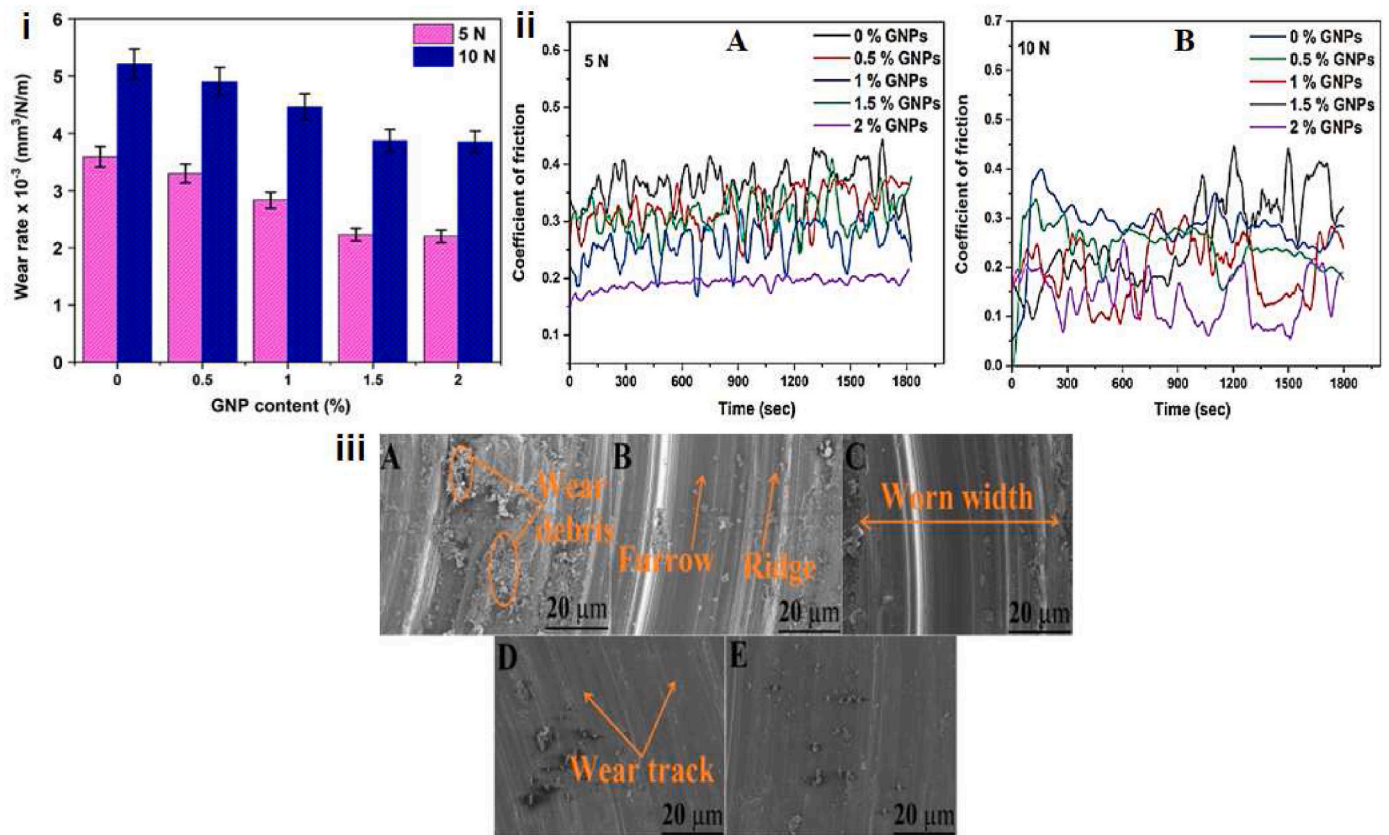


Fig. 8. Tribology properties of the sintered Mg-based AZ91D-Ni alloy and AZ91Mg-Ni-GNPs composites. (i) wear rate under the load of 5 and 10 N, (ii) friction coefficient versus time under loads of (a) 5 N and (b) 10 N, and (iii) wear surface morphology under the load of 10 N for samples a-e.

composite grade. Therefore, the results reveal that the presence of GNPs in the AZ91D-Ni-GNPs Mg-based composite grade compared to the AZ91-Ni alloy grade improves the stiffness effect of the developed components.

3.4.3. Wear behaviour of the sintered Mg-based AZ91D-Ni alloy and AZ91D-Ni-GNPs composites

The wear test is conducted under two separate loads to understand the performance of the sintered Mg-based AZ91D-Ni alloy and AZ91D-Ni-GNPs composites. The resulting performances under different loads are shown in Fig. 8I. Similarly, the coefficient of friction for the two loads are shown in Fig. 8(II) a (5 N load) and b (10 N load). It is noticed that the wear rate of the sintered AZ91D-Ni alloy is remarkably higher compared to the sintered AZ91D-Ni-GNPs composites at the two operating loads. However, minimal differences are noticed in the behaviour of sintered composite with 1.5 and 2 wt% GNPs reinforcement. The wear rate values for the two grades of Mg-based composite, i.e., 1.5 and 2 wt% GNPs reinforcement, are 2.23×10^{-3} (1.5 wt%, 5 N load), 3.87×10^{-3} (1.5 wt%, 10 N load), 2.2×10^{-3} (2 wt%, 5 N load) and 3.85×10^{-3} mm³/N/m (2 wt%, 10 N load), respectively. A similar trend is noticed in the microhardness behaviour of the two AZ91D-Ni-GNPs composites. The highest wear rate values are 3.59×10^{-3} (0 wt%, 5 N load) and 5.21×10^{-3} mm³/N/m (0 wt%, 10 N load) obtained in AZ91D-Ni Mg alloy. The microhardness of the AZ91D-Ni-GNPs composites increases with an increase in the weight percent of GNP and accordingly increases the wear resistance of the composites. This behaviour is in agreement with Archard's law [42,43]. Additionally, the high-strength GNPs reinforcement in soft AZ91D-Ni alloy increases the load-bearing capability of the sintered AZ91D-Ni-GNPs composites and consequently improves the work-hardening ability by entrapping dislocations [44,45].

Thus, the role of the high-strength GNPs in Mg alloy yields better

wear resistance properties because it enables the test samples (composite) to withstand the penetration of the counter surface asperities into it [46]. The reduced wear rate values obtained at a lower load result from the frictional heating oxide debris filling the surface of the test samples and, in turn, forming a tribolayer which reduces the wear rate. At higher loads, thermal softening occurred at the contact point between the counter surface and test samples, leading to the braking of the tribolayer and, in succession, increasing the wear rate. While the heat generated due to dry-sliding wear testing increases the surface temperature of the test samples, leading to plastic deformation by thermal softening in the alloy, the addition of GNPs prolongs the thermal effect in the composites and helps to form a protective oxidised layer [11] quickly. The impact of the Mg₁₇Al₁₂ strengthening phase is noteworthy, although not quantified. This strengthening phase also contributes to the enhanced properties displayed by the sintered AZ91D-Ni-GNPs composites. However, the discussion around whether it is a brittle or ductile phase is subject to debate because it is still ongoing in the literature [47]. Consequently, the observations recorded imply that GNPs can serve as a good nanoparticle reinforcement in Mg-based alloys.

Fig. 8(II) represents the variation obtained for the coefficient of friction (COF) versus time at two different loads of 5 and 10 N. It is observed from Fig. 8(II) a and b that a steady-state coefficient of friction is recorded for all the samples under the two loads utilised. It ranges from 0.17 to 0.4 for a 5 N load and 0.06 to 0.45 for a 10 N load. The COF's fluctuating pattern displayed for AZ91D-Ni alloy and AZ91D-Ni-GNPs composite grades is similar, even when the load is raised from 5 to 10 N. Nevertheless, the fluctuation behaviour could result from the activities of the wear debris generated due to the movement of the counterface ball on the test piece, and the impact of the loads utilised [48]. While most wear debris is removed from the worn surface, few remain trapped and form a plateau on the wear track with a high substance of metal oxides, thus offering a lubricating effect that results in a

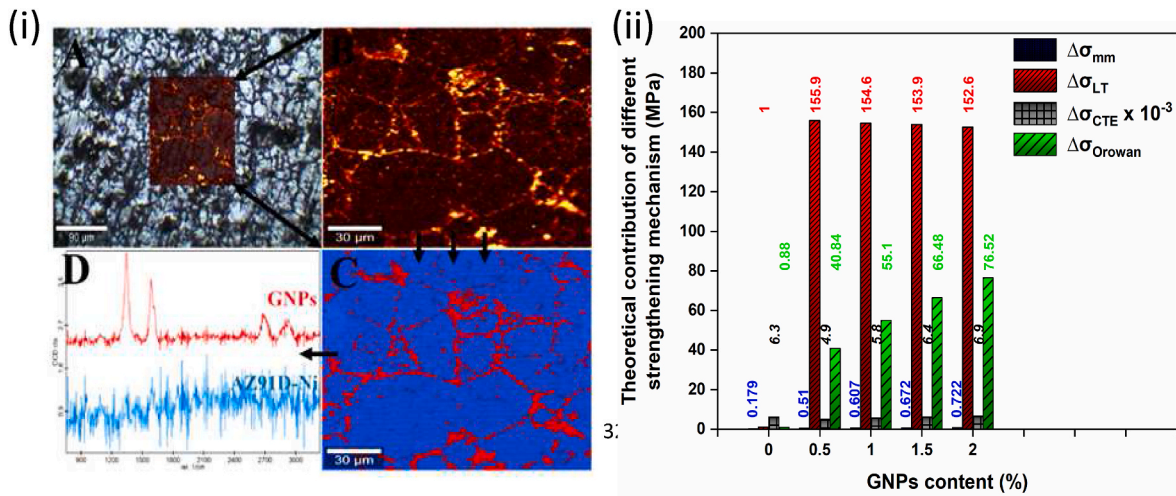


Fig. 9. Raman spectroscopy images and the increasing GNPs content (wt%) against the theoretically calculated contribution of each strengthening mechanism: (Ia) Microstructure image of 2 wt% GNPs reinforced AZ91D-Ni alloy, (Ib) Morphology of the mapped area, (Ic) Identification of matrix and reinforcement phases using colour code, (Id) Raman spectra confirming the presence/behaviour of the matrix and GNPs reinforcement. (II) The behaviour of increasing GNPs content (wt%) against the theoretically calculated contribution of each strengthening mechanism.

low range of COF values. Overall, the least coefficient of friction is observed with 2 wt% GNPs reinforcement, thus suggesting that increasing the GNPs constituent in AZ91D-Ni alloy could reduce grain size and increase strength, thereby improving the wear resistance considerably. The results observed in this study are in agreement with the work reported by Shahin M. et al. [49], indicating that GNPs reinforced Mg alloy promises higher potential wear resistance than AZ91D [50], and AZ91D-Ni alloys [8,9] wear properties.

3.4.4. Wear track analysis of the sintered Mg-based AZ91D-Ni alloy and AZ91D-Ni-GNPs composites

Fig. 8(III) presents the wear tracks' SEM images of the worn areas of the sintered Mg-based AZ91D-Ni and AZ91D-Ni-GNPs composites under 10 N load during wear analysis. The wear debris along the wear track is more pronounced in the alloy without GNPs, while it reduces with an increase in GNPs reinforcement. This corroborates the low wear resistance observed in composites with GNPs reinforcement (Fig. 8I). Adding GNPs in the AZ91D-Ni alloy enhances the wear resistance and plastic deformation during sliding wear testing of AZ91D-Ni-GNPs Mg-based composite grades, alongside contributing to grain refinement of the Mg matrix. The formation of furrows and ridges along the wear tracks are prominent in the materials with low GNPs content, i.e., an increase in GNPs minimises the formation of furrows (grooves). Similarly, it could be realised that the depth of furrows and height of ridges reduce with an increase in the amount of GNPs in the AZ91D-Ni alloy, suggesting that materials with a considerably high constituent of GNPs possess better wear resistance properties. The display of high wear resistance behaviour for the sintered Mg-based AZ91D-Ni-GNPs composite grades during dry-sliding wear testing can be attributed to numerous factors [49], such as the; (i) contribution of the self-lubrication effect of GNPs; (ii) increase hardness of AZ91D-Ni-GNPs composite resulting from the addition of Ni to AZ91D alloy [8]; (iii) high stiffness property of GNPs (~ 1 TPa) which to some extent is capable of lowering the tangential force during sliding by the counterface material; and (iv) dispersion of GNPs reinforcement in the AZ91D-Ni matrix which can reduce delamination of the oxide tribolayer, formed [51,52].

4. Strengthening mechanism in the sintered Mg-based AZ91D-Ni-GNPs composites

In place of a schematic representation of the strengthening mechanism that occurs in the addition of GNPs to the AZ91D-Ni Mg alloy,

Fig. 9I (Raman spectroscopy analysis) images illustrate the formation of GNPs within the microstructure of the sintered composite, thus leading to the enhancements in the mechanical properties of GNPs reinforced AZ91D-Ni Mg alloy. Fig. 9(II) shows the calculated values of $\Delta\sigma_{Hall-Petch}$, $\Delta\sigma_{LT}$, $\Delta\sigma_{CTE}$, $\Delta\sigma_{mm}$ and $\Delta\sigma_{Orowan}$ strengthening mechanism for AZ91D-Ni-GNPs Mg-based composites with varied GNPs content from 0 to 2 wt% at 0.5 wt% GNPs increment. The improvement observed in the composites can be attributed to the excellent strengthening characteristics/properties of GNPs, relatively homogenous dispersion of GNPs combined with the superior structural integrity that GNPs possess, and strong interfacial metallurgical bonding produced between GNPs and AZ91D-Ni Mg alloy. Accordingly, the strengthening mechanisms resulting in an enhancement in the developed GNPs reinforced Mg-based composites grade are summaries thus; (I) grain refinement ($\Delta\sigma_{Hall-Petch}$) because of heterogeneous nucleation of AZ91D-Ni Mg alloy on the GNPs reinforcement, (II) beneficial load transfer from AZ91D-Ni Mg alloy to GNPs reinforcement ($\Delta\sigma_{LT}$), (III) formation of dislocations due to the mismatch in the coefficient of thermal expansion (CTE) ($\Delta\sigma_{CTE}$), (IV) strengthening through modulus mismatch ($\Delta\sigma_{mm}$), and (V) Orowan strengthening ($\Delta\sigma_{Orowan}$) due to the GNPs impeding dislocation motion. According to Rashad M. et al. [41], the mechanisms mentioned can be used to express the yield strength of the AZ91-Ni-GNPs Mg-based composite; thus, equation (1):

$$\sigma_c = \sigma_m + \Delta\sigma_{Hall-Petch} + \Delta\sigma_{LT} + \Delta\sigma_{CTE} + \Delta\sigma_{mm} + \Delta\sigma_{Orowan} \quad (1)$$

where σ_c is the yield strength of the AZ91D-Ni-GNPs composite, σ_m represent the yield strength of the AZ91D Mg alloy (matrix), $\Delta\sigma_{Hall-Petch}$ represent the enhancement in the yield strength as a result of the reduction in grain size, $\Delta\sigma_{LT}$ represent the enhancement as a result of load transfer between matrix alloy and nanoparticle reinforcement, $\Delta\sigma_{CTE}$ represent the enhancement produced as a result of a mismatch between the GNPs reinforcement, $\Delta\sigma_{mm}$ is the enhancement due to modulus mismatch between reinforcement and AZ91-Ni matrix, and $\Delta\sigma_{Orowan}$ represent the improvement due to Orowan strengthening. From the expression above, the in-situ growth and non-uniform nucleation of AZ91-Ni alloy on GNP reinforcement decrease grain size in the sintered composites. Moreover, the increase in the development of refined grains resulting from the nucleation of the Mg matrix on GNPs reinforcement increases the number of grain boundaries developed. This invariably increases the rate at which dislocation motion is reduced. By so doing, the yield strength of the sintered AZ91D-Ni-GNPs slightly increases following the Hall-Petch relation in equation (2) [33].

$$\Delta\sigma_{Hall-Petch} = K \left(d_{composite}^{-1/2} - d_{matrix}^{-1/2} \right) \quad (2)$$

where $d_{composite}$ and d_{matrix} represent the average grain sizes of the AZ91D-Ni-GNPs composites and AZ91D-Ni matrix, respectively. In this study, the average grain size of the composites with 0.5, 1, 1.5 and 2 wt % GNPs are 26.29, 25.99, 24.91 and 23.35 μm , respectively, while the alloy without GNPs is 26.91 μm . K represents the Hall-Petch coefficient of the Mg matrix. Due to the closeness in the average grain size of the sintered components and according to Parizi M. et al. and Li P. et al. [33, 53], the significant contribution of $\Delta\sigma_{Hall-Petch}$ strengthening mechanism (grain refinement) could be ignored. Thus, this does not apply in this study. Therefore, the yield strength of the sintered components expressed in equation (1) is reduced to equation (3) as follows:

$$\sigma_c = \sigma_m + \Delta\sigma_{LT} + \Delta\sigma_{CTE} + \Delta\sigma_{mm} + \Delta\sigma_{Orowan} \quad (3)$$

The load transfer ($\Delta\sigma_{LT}$) mechanism describes the phenomenon where shear stress is transferred from the Mg matrix alloy to the matrix/reinforcement interface and subsequently to the Ni/GNPs reinforcements. Thus, for an effective load transfer to occur, strong interfacial metallurgical bonding between the Ni/GNPs reinforcements and Mg matrix should exist. In this study, the relative density and microstructural properties display high densification, reduced porosity, and the $\text{Mg}_{17}\text{Al}_{12}$ phase (XRD) formation. This implies strong metallurgical bonding between the Mg matrix and Ni/GNPs reinforcement exists. It occurred through the formation of nanoscale contact between Ni/GNPs and Mg matrix aided by the irregular shape of the GNPs in the development of spark plasma sintered Mg-based AZ91D-Ni-GNPs composite grade. The irregular shape of the GNPs possesses large surface areas that help in the formation of an interlocked bonding interface between the sunken and raised edges of the GNPs and the surrounding Mg crystalline grains [40]. Consequently, it promotes the formation of mechanical micro-occlusion [40,54], which improves the metallurgical bonding formed at the interface between GNPs reinforcement and Mg matrix, leading to effective load transfer and improvement of the mechanical properties in the sintered Mg-based AZ91D-Ni-GNPs composite. Therefore, the strengthening mechanism of load transfer in the sintered composited from Mg matrix to Ni/GNPs reinforcement can be assessed by employing the following, adapted shear lag model in equation (4) [55]:

$$\Delta\sigma_{LT} = V_r \left(\frac{S}{A} \right) \left(\frac{\tau_m}{2} \right) + \sigma_m V_m \quad (4)$$

where V_r and V_m represent the fractional volume of the Ni/GNPs reinforcement and Mg matrix, respectively, A and S represent the cross-sectional areas and interfacial of the GNPs reinforcement, which can be written as $2(t + d_r) \times d_r$ and $t \times d_r$, respectively, where t and d_r are the average thickness and length of GNPs reinforcement, respectively, σ_m and τ_m represent the yield strength and shear strength of the Mg matrix, respectively, and τ_m can be simplified in the form of $1/2 \sigma_m$. In addition, the Ni inclusion contributes to the strength improvement through the load-bearing strengthening mechanism, and this is evaluated using a modified shear lag model in equation (5) [56]:

$$\Delta\sigma_{LT} = 0.5\sigma_m V_r S_e \quad (5)$$

where $S_e = 1$ for a spherical reinforcement [56]. Thus, the calculated $\Delta\sigma_{LT}$ for 1.5 wt% Ni (70 MPa) is 1 MPa, which is significantly smaller compared to the strengthening contribution from GNPs.

The CTE of AZ91D Mg alloy is $25.2 \times 10^{-6} \text{ K}^{-1}$ [53,57], GNPs reinforcement is $1 \times 10^{-6} \text{ K}^{-1}$ [33], and Ni CTE is $12 \times 10^{-6} \text{ K}^{-1}$ [58]. According to Sun X. et al. [59], it may be inferred that the large difference in the CTE between the AZ91D Mg matrix and Ni/GNPs reinforcement will result in the formation of local strain in the structure of the composite due to thermal mismatch and subsequently dislocations at the matrix-reinforcement interface. The increasing formation of

dislocations at the matrix-reinforcements interface equally contributes to the increase in the yield strength of the sintered AZ91D-Ni-GNPs composite grade, although not significant. Therefore, the $\Delta\sigma_{CTE}$ which represents the enhancement produced as a result of the coefficient of thermal mismatch between the Ni/GNPs reinforcements and AZ91D Mg matrix can be estimated following equation (6) [59]:

$$\Delta\sigma_{CTE} = \alpha G b \sqrt[4]{8 \frac{V_r \times (\Delta C \times \Delta T)}{b d_r}} \quad (6)$$

where α is a geometric constant (1.25), G represent the shear elastic modulus of the AZ-91D-Ni matrix, b denotes the Burgers vector of the AZ91D Mg matrix, V_r represent the volume of reinforcement, ΔC represents the CTE variation between the Ni/GNPs reinforcement and AZ91D matrix, ΔT denotes the variation between the SPS temperature and room temperatures, and d_r represent the average size of the Ni/GNPs reinforcement.

Furthermore, the enhancement contribution of Ni/GNPs through strengthening mechanism due to modulus mismatch is calculated following equation (7), thus [33]:

$$\Delta\sigma_{MM} = \alpha G b \sqrt[4]{\frac{G V_r}{b r}} \quad (7)$$

where α , G , b and V_r are the same as earlier stated, while r is the half-length and particle size of Ni/GNPs reinforcements.

Similarly, the Orowan strengthening correspondingly plays a critical role as part of the strengthening mechanism that ensued in improving the AZ91D-Ni-GNPs composite. The presence of Ni/GNPs in the AZ91D Mg matrix aids the formation of residual dislocation loops in the region surrounding the Ni/GNPs, especially when dislocations in the AZ91D Mg matrix permeate through Ni/GNPs reinforcements during deformation. Back stress is produced in the process, which inhibits the migration of dislocations and increases the yield strength of the sintered AZ91D-Ni-GNPs Mg-based composite grade. The Orowan strengthening can be expressed as follows in equation (8) [4]:

$$\Delta\sigma_{Orowan} = \frac{0.13 G b}{d_r \left[\left(\frac{1}{2v_r} \right)^{1/3} - 1 \right]} \cdot \ln \left(\frac{d_r}{2b} \right) \quad (8)$$

where G , b , d_r and v_r represent the quantities in equation (6).

Summarily, the four strengthening mechanisms, apart from $\Delta\sigma_{Hall-Petch}$ observed in this study can be utilised to compute the yield strength of the sintered AZ91D-Ni-GNPs Mg-based composite grade with varied GNPs. The calculated values of the $\Delta\sigma_{mm}$, $\Delta\sigma_{LT}$, $\Delta\sigma_{CTE}$, and $\Delta\sigma_{Orowan}$ for the AZ91D-Ni-GNPs composites at 0–2 wt % GNPs are presented in Fig. 9(II). These are 0.179, 0.510, 0.607, 0.672 and 0.722 MPa, respectively, for modulus mismatch ($\Delta\sigma_{mm}$) of GNPs reinforcement between 0 and 2 wt%. The load transfer ($\Delta\sigma_{LT}$) strengthening mechanism values with respect to the increasing reinforcement from 0 to 2 wt% are 0, 136.87, 135.58, 134.89, and 133.55 MPa, respectively, while that of Ni is 1 MPa. The strengthening mechanism values with respect to $\Delta\sigma_{CTE}$ are 0.0063, 0.0049, 0.0058, 0.0064, and 0.0069 MPa, respectively, with an increase in GNPs reinforcement from 0 to 2 wt%. The $\Delta\sigma_{Orowan}$ strengthening mechanism is equally observed, and the values recorded in relation to the increasing GNPs reinforcement from 0 to 2 wt% are 0.88, 40.84, 55.10, 66.48 and 76.52 MPa, respectively. The yield strength (σ_m) of AZ91D Mg alloy is 158 MPa [56,60]. Therefore, for the 0, 0.5, 1, 1.5 and 2 wt% GNPs in Mg-based AZ91D-Ni-GNPs composite grade, the summation of the contribution of the calculated load transfer, thermal mismatch, modulus mismatch and Orowan strengthening to the improvement of the theoretical yield strength (σ_c) according to equation (3), are 140.06, 316.22, 329.29, 340.05 and 348.80 MPa, respectively. The main strengthening factors among the five strengthening mechanisms observed in the fabricated

Table 2

The theoretical calculations of various strengthening mechanisms for sintered Mg-based AZ91D-Ni-GNPs composites grade.

Sample	σ_m (MPa)	$\Delta\sigma_{mn}$ (MPa)	$\Delta\sigma_{LT}$ (MPa)	$\Delta\sigma_{CTE} \times 10^{-3}$ (MPa)	$\Delta\sigma_{Orowan}$ (MPa)	σ_c (MPa)
AZ91D-1.5Ni	138	0.179	1	6.3	0.88	140.0653
AZ91D-1.5Ni-0.5GNPs	138	0.510	155.9	4.9	40.84	316.2249
AZ91D-1.5Ni-1GNPs	138	0.607	154.6	5.8	55.10	329.2928
AZ91D-1.5Ni-1.5GNPs	138	0.672	153.9	6.4	66.48	340.0484
AZ91D-1.5Ni-2GNPs	138	0.722	152.6	6.9	76.52	348.7989

Table 3

Essential values for calculating the strengthening mechanisms.

V_r (%)	d_r (m)	CTE of GNPs (K^{-1})	ΔC	G (MPa)	b (m)	CTE of AZ91D (K^{-1})
0–2.0	1.5×10^{-8}	1×10^{-6} [54]	2.41×10^{-5} (GNP) [41]	1.66×10^4 [41]	3.21×10^{-10} [41]	25.1×10^{-6} [41]
			1.21×10^{-5} (Ni)			
V_m (%)	CTE of Ni	t (μm)	σ_m (MPa)	ΔT (k)	α	
96.5–98.5	$13 \times 10^{-6} K^{-1}$ [57]	5	158 [55,59]	648 [41]	1.25 [54]	

Mg-based composites are the load transfer followed by the Orowan strengthening. In the estimation of the theoretical strength of the sintered composites, the load transfer strengthening has the highest contribution, with the highest value obtained with the composite reinforced with 2 wt% GNPs. In Fig. 9I, it can be seen that the GNPs reinforcement primarily resided at the grain boundary interface, which significantly facilitates the load transfer mechanism, followed by Orowan strengthening, while the inclusion of Ni mainly strengthens the AZ91D alloy through load transfer. The value showing the contribution of each strengthening mechanism in the total improvement of the yield strength of AZ91-Ni-GNPs composites grade is provided in Fig. 9(II). Generally, the increase in the constituent of GNPs reinforcement results in an increase in strengthening mechanisms that formed in the sintered composites from 0.5 wt% GNPs to 2 wt% GNPs reinforced Mg-based composite. Minimal improvement was observed with the 0 wt% Mg-based alloy compared to the composites. Table 4 compares the contribution of individual strengthening mechanisms and their calculated total theoretical yield strength of similar Mg-based composite studies reported in the literature with the findings in this study. As indicated earlier, the hybrid reinforcement of AZ91D Mg-based alloy

Table 4

Comparison of previous studies with the findings (in this study) in terms of the contribution of individual strengthening mechanisms and their calculated theoretical yield strength of Mg-based reinforced carbonaceous materials.

Sample	σ_m (MPa)	$\Delta\sigma_{H-P}$	$\Delta\sigma_{mn}$ (MPa)	$\Delta\sigma_{LT}$ (MPa)	$\Delta\sigma_{CTE} \times 10^{-3}$ (MPa)	$\Delta\sigma_{Orowan}$ (MPa)	σ_c (MPa)	Ref.
AZ91D-2.7Mg ₂ Si-0.1CNTs	158.4	–	–	15.8	68.1	29.6	234.3	[53]
AZ91D-2.7Mg ₂ Si-0.3CNTs	158.4	–	–	43.3	75.7	30.7	250.9	[53]
AZ91D-2.7Mg ₂ Si-0.5CNTs	158.4	–	–	70.8	76.8	31.5	267.5	[53]
0.3CNTs-1.2Mg ₂ Si _p /Mg	–	–	–	41.8	81.5	28.6	234.0	[60]
0.75CNTs-0.75Mg ₂ Si _p /Mg	–	–	–	103.0	75.9	24.2	268.2	[60]
1.5CNTs/Mg	–	–	–	204.9	32.7	4.2	345.6	[60]
1.5Mg ₂ Si _p /Mg	–	–	–	1.0	75.0	29.0	218.4	[60]
Mg-0.05GNPs	133	1.7	–	28.1	6.2	–	169	[62]
Mg-0.1GNPs	133	3.9	–	58.3	8.8	–	204	[62]
Mg-0.15GNPs	133	7.1	–	90.2	10.7	–	241	[62]
Mg-1.5GNPs	124.7	17.8	–	35.4	28.6	7.9	214.4	[40]
AZ91D-1.5Ni	138	–	0.179	1	6.3	0.88	140.07	This work
AZ91D-1.5Ni-0.5GNPs	138	–	0.510	155.9	4.9	40.84	316.22	This work
AZ91D-1.5Ni-1GNPs	138	–	0.607	154.6	5.8	55.10	329.29	This work
AZ91D-1.5Ni-1.5GNPs	138	–	0.672	153.9	6.4	66.48	340.05	This work
AZ91D-1.5Ni-2GNPs	138	–	0.722	152.6	6.9	76.52	348.80	This work

results in significant overall improvement of the composites. Thus, this study implies that adding reinforcement, especially GNPs, to AZ91D Mg-based alloy significantly enhances the yield strength in the sintered high-performance AZ91D-Ni-GNPs grade composite [61]. Tables 2 and 3 present the summary of the contribution of each strengthening mechanism, the summation of the strengthening mechanisms in obtaining the calculated yield strength of the sintered Mg-based composite grade and the essential values for calculating the strengthening mechanisms (see Table 4).

5. Conclusions

In this study, high-performance Mg-based AZ91D-Ni-GNP composites with varied GNPs reinforcement were effectively fabricated through the effective activation of GNPs and spark plasma sintering technology. The homogenous distribution of Ni and GNPs powders in the AZ91D powder is realised. As an alloying element, Ni stimulates grain-refinement consequence to the metal matrix composites, and the addition of GNPs further improves the grain-refinement and enhances the strength of the sintered composites through different synergetic strengthening mechanisms. The mechanism includes grain refinement, thermal mismatch, load transfer, modulus mismatch and Orowan strengthening. Through the analyses of the microstructure utilising SEM, EDS, XRD, Raman spectroscopy and mechanical/tribology properties using micro/nano hardness, elastic modulus and wear rate, the following conclusions were drawn:

1. The addition of Ni and GNPs reinforcement to AZ91D matrices results in considerable enhancement of the properties of the sintered composites through synergetic strengthening mechanisms.
2. The micro/nano hardness, elastic modulus, and wear rate of the sintered composites were higher compared to the AZ91D-Ni alloy sample, displaying the positive contribution of GNPs reinforcement to the improvement of the mechanical/tribological properties of the AZ91D Mg matrices.

- The addition of Ni and GNPs reinforcement in AZ91D matrices assists in reducing plastic deformation during sliding wear testing and promotes grain refinement of the Mg matrices, leading to an improved wear rate with an increase in reinforcement constituents.
- The load transfer and Orowan strengthening mechanisms were the dominant and primary mechanisms contributing to the improved yield strength of the sintered metal matrix composites.
- Considering the effective and optimistic contribution of the reinforcement, especially GNPs, in the improvement of the properties of AZ91D Mg-based alloy, this study encourages additional studies to investigate the optimum reinforcement concentrations in the AZ91D alloy matrix and the biocompatibility of the sintered AZ91D-Ni-GNPs composite grade.

CRedit authorship contribution statement

Olugbenga Ogunbiyi: Conceptualization, Formal analysis, Data curation, Writing – original draft. **Samuel A. Iwarere:** Conceptualization, Formal analysis, Data curation, Writing – review & editing. **Rotimi Sadiku:** Conceptualization, Writing – review & editing. **Michael O. Daramola:** Conceptualization, Formal analysis, Data curation, Writing – review & editing.

Declaration of competing interest

The authors declare no competing financial interest or personal relationships that could have appeared to influence the work reported in this paper.

Acknowledgements

The authors acknowledge the financial support for this research by the Department of Chemical Engineering of the University of Pretoria and the Faculty of Engineering, the Built Environment and Information Technology, Pretoria, South Africa. The authors also thank the scientific and technical assistance from the Faculty of Natural and Agricultural Sciences Laboratory for Microscopy and Microanalysis, the University of Pretoria and the Institute for Nano-Engineering Research, Department of Chemical, Metallurgical and Materials Engineering of the Tshwane University of Technology, Pretoria, South Africa.

Appendix A. Supplementary data

Supplementary data to this article can be found online at <https://doi.org/10.1016/j.jmrt.2024.02.027>.

References

- Pu-Bo Li, Tan Wan-Ting, Gao Mang-Mang, Liu Kuan-Guan. Semisolid microstructural evolution of (CNTs+ Si p)/AZ91D powder compacts prepared from powders by cold pressing and remelting. *Rare Metals* 2020;39:733–42.
- Vahedi F, Zarei-Hanzaki A, Salandari-Rabori A, Razaghian A, Abedi HR, Minarik P. Texture evolution and wear properties of a frictionally stir processed magnesium matrix composite reinforced by micro graphite and nano graphene particles. *Mater Res Express* 2019;6(10):1065–6.
- Pan Fusheng, Yang Mingbo, Chen Xianhua. A review on casting magnesium alloys: modification of commercial alloys and development of new alloys. *J mater sci technol* 2016;32(12):1211–21.
- Munir Khurram, Wen Cuie, Li Yuncang. Graphene nanoplatelets-reinforced magnesium metal matrix nanocomposites with superior mechanical and corrosion performance for biomedical applications. *J Magnes Alloy* 2020;1(8):269–90.
- Rashad Muhammad, Pan Fusheng, Hu Huanhuan, Asif Muhammad, Hussain Shahid, Jia She. Enhanced tensile properties of magnesium composites reinforced with graphene nanoplatelets. *Mater Sci Eng A* 2015;630:36–44.
- Chen Liwen, Zhao Yuhong, Hou Hua, Zhang Ting, Liang Jianquan, Li Muxi, Jing Li. Development of AZ91D magnesium alloy-graphene nanoplatelets composites using thixomolding process. *J Alloys Compd* 2019;778:359–74.
- Ogunbiyi Olugbenga, Iwarere Samuel A, Daramola Michael O. Empirical prediction of optimum process conditions of spark plasma-sintered magnesium composite (AZ91D-Ni-GNPs) using response surface methodology (RSM) approach. *Arab J Sci Eng* 2023;48(3):3041–59.
- Hassan S Fida, Nasirudeen OO, Al-Aqeeli N, Saheb N, Patel F, M. M. A. Baig. Magnesium–nickel composite: preparation, microstructure and mechanical properties. *J Alloys Compd* 2015;646:333–8.
- Olalekan Ogunlakin Nasirudeen, Abdul Samad M, Hassan Syed Fida, Ibrahim Elhady Muhammad Mohamed. Tribological evaluations of spark plasma sintered Mg–Ni composite. *Tribol - Mater Surf Interfaces* 2022;16(2):110–8.
- Olalekan Ogunlakin Nasirudeen, Abdul Samad M, Hassan Syed Fida, Ibrahim Elhady Muhammad Mohamed. Tribological evaluations of spark plasma sintered Mg–Ni composite. *Tribol - Mater Surf Interfaces* 2022;16(2):110–8.
- Li Xuejian, Shi Hailong, Wang Xiaojun, Hu Xiaoshi, Xu Chao, Shao Wenzhu. Achieving high strength and ductility in GNSs/Mg nanocomposites fabricated by in-situ liquid metallurgy combined with hot extrusion. *Compos Part A Appl Sci Manuf* 2022;161:107079.
- Shahin Mohammad, Munir Khurram, Wen Cuie, Li Yuncang. Magnesium-based composites reinforced with graphene nanoplatelets as biodegradable implant materials. *J Alloys Compd* 2020;828:154461.
- Yang Yan, Xiong Xiaoming, Chen Jing, Peng Xiaodong, Chen Daolun, Pan Fusheng. Research advances of magnesium and magnesium alloys worldwide in 2022. *J Magnes Alloy* 2023;11(8):2611–54.
- Ogunbiyi Olugbenga, Sadiku Rotimi, Adesina Oluwagbenga, Adesina Olanrewaju Seun, Smith Salifu, Fayomi Juwon. Microstructure and mechanical properties of spark plasma-sintered graphene-reinforced Inconel 738 low carbon superalloy. *Metall Mater Trans* 2022;53:299–313.
- Ogunbiyi Olugbenga, Jamiru Tamba, Sadiku Rotimi, Adesina Oluwagbenga, Adesina Olanrewaju Seun, Obadele Babatunde Abiodun. Spark plasma sintering of graphene-reinforced Inconel 738LC alloy: wear and corrosion performance. *Met Mater Int* 2020:1–15.
- Shahin Mohammad, Wen Cuie, Munir Khurram, Li Yuncang. Mechanical and corrosion properties of graphene nanoplatelet–reinforced Mg–Zr and Mg–Zr–Zn matrix nanocomposites for biomedical applications. *J Magnes Alloy* 2022;10(2):458–77.
- Kavimani V, Soorya Prakash K, Titus Thankachan. Investigation of graphene-reinforced magnesium metal matrix composites processed through a solvent-based powder metallurgy route. *Bull Mater Sci* 2019;42:1–9.
- Oketola Adeola, Jamiru Tamba, Taoreed Adegbola Adesola, Ogunbiyi Olugbenga, Sadiku Rotimi, Smith Salifu. Influence of sintering temperature on the microstructure, mechanical and tribological properties of ZrO2 reinforced spark plasma sintered Ni–Cr. *Int j lightweight mater manuf* 2022;5(2):188–96.
- Ogunbiyi OF, Sadiku ER, Jamiru T, Adesina OT, Beneke LW. Spark plasma sintering of Inconel 738LC: densification and microstructural characteristics. *Mater Res Express* 2019;6(10):1065–8.
- Wall M. The Raman spectroscopy of graphene and the determination of layer thickness. *Thermo Sci* 2011;5:1–5.
- ASTM. E2546 - 15 standard practice for instrumented indentation testing. 2023. <http://www.astm.org/e2546-15.html>.
- Dada M, Popoola P, Mathe N, Adeosun S, Pityana S. Investigating the elastic modulus and hardness properties of a high entropy alloy coating using nanoindentation. *Int j lightweight mater manuf* 2021;4(3):339–45.
- ASTM standard test method for wear testing with a pin-on-disc apparatus. In: *Astm G99-95*; 1995. Philadelphia, PA.
- Nikmardan Somayeh, Pouyafar Vahid. Fabrication of AZ91D/SiCp composites by mechanical milling of magnesium alloy chips and spark plasma sintering in a semi-solid regime. *J Asian Ceram Soc* 2019;7(2):154–60.
- Mondet M, Barraud E, Lemonnier S, Guyon J, Allain N, Grosdidier T. Microstructure and mechanical properties of AZ91 magnesium alloy developed by Spark Plasma Sintering. *Acta Mater* 2016;119:55–67.
- Obadele Babatunde Abiodun, Oladeji Oluremi Ige, Peter Apata Olubambi. Fabrication and characterization of titanium-nickel-zirconia matrix composites prepared by spark plasma sintering. *J Alloys Compd* 2017;710:825–30.
- Yuan Qiu-hong, Zhou Guo-hua, Liao Lin, Liu Yong, Luo Lan. Interfacial structure in AZ91 alloy composites reinforced by graphene nanosheets. *Carbon* 2017;127:177–86.
- Minarik Peter, Stráský Josef, Veselý Jozef, František Lukáč, Hadzima Branislav, Kral Robert. AE42 magnesium alloy prepared by spark plasma sintering. *J Alloys Compd* 2018;742:172–9.
- Ogunbiyi Olugbenga, Sadiku Rotimi, Adesina Oluwagbenga, Olanrewaju Seun Adesina, Smith Salifu, Fayomi Juwon. Microstructure and mechanical properties of spark plasma-sintered graphene-reinforced Inconel 738 low carbon superalloy. *Metall Mater Trans A* 2022;53:299–313.
- Fan Yuchao, Ye Li, Tian Qingyong, Zhuang Yuanlin, Zhang Yingjiu, Li Xinjian. Effects of aligned graphene sheets on mechanical properties of ZK61 alloy. *Mater Sci Eng A* 2021;801:140417.
- Muhammad Wan Nur Azrina Wan, Sajuri Zainuddin, Mutoh Yoshiharu, Miyashita Yukio. Microstructure and mechanical properties of magnesium composites prepared by spark plasma sintering technology. *J Alloys Compd* 2011;509(20):6021–9.
- Rashad Muhammad, Pan Fusheng, Tang Aitao, Asif Muhammad, Aamir Muhammad. Synergetic effect of graphene nanoplatelets (GNPs) and multi-walled carbon nanotube (MW-CNTs) on mechanical properties of pure magnesium. *J Alloys Compd* 2014;603:111–8.
- Parizi M Torabi, Ebrahimi GR, Ezatpour HR. Effect of graphene nanoplatelets content on the microstructural and mechanical properties of AZ80 magnesium alloy. *Mater Sci Eng A* 2019;742:373–89.
- Zhu Yunpeng, Qin Jiayu, Wang Jinhui, Jin Peipeng. Effect of sintering temperature on microstructure and mechanical properties of AZ91 magnesium alloy via spark plasma sintering. *Adv Eng Mater* 2022;24(3):2100905.

- [35] Rashad Muhammad, Pan Fusheng, Zhang Jianyue, Asif Muhammad. Use of high energy ball milling to study the role of graphene nanoplatelets and carbon nanotubes reinforced magnesium alloy. *J Alloys Compd* 2015;646:223–32.
- [36] Zhou MY, Ren LB, Fan LL, Tun KS, Gupta M, Zhang YWX, Lu TH, Quan GF. Achieving ultra-high strength and good ductility in AZ61 alloy composites containing hybrid micron SiC and carbon nanotubes reinforcements. *Mater Sci Eng A* 2019;768:138447.
- [37] Guerra Valentina, Wan Chaoying, Degirmenci Volkan, Sloan Jeremy, Presvytis Dimitris, Watson Michael, McNally Tony. Characterisation of graphite nanoplatelets (GNP) prepared at scale by high-pressure homogenisation. *J Mater Chem C* 2019;7(21):6383–90.
- [38] Munir Khurram S, Wen Cuie. Deterioration of the strong sp² carbon network in carbon nanotubes during the mechanical dispersion processing—a review. *Crit Rev Solid State Mater Sci* 2016;41(5):347–66.
- [39] Turan Muhammet Emre, Sun Yavuz, Akgul Yasin, Turen Yunus, Ahlatci Hayrettin. The effect of GNPs on wear and corrosion behaviors of pure magnesium. *J Alloys Compd* 2017;724:14–23.
- [40] Sun Xueyu, Li Chaojie, Dai Xibin, Zhao Lixin, Li Baoye, Wang Hongshui, Liang Chunyong, Li Haipeng, Fan Jiawei. Microstructures and properties of graphene-nanoplatelet-reinforced magnesium-matrix composites fabricated by an in situ reaction process. *J Alloys Compd* 2020;835:155125.
- [41] Rashad Muhammad, Pan Fusheng, Asif Muhammad, Tang Aitao. Powder metallurgy of Mg–1% Al–1% Sn alloy reinforced with low content of graphene nanoplatelets (GNPs). *J Ind Eng Chem* 2014;20(6):4250–5.
- [42] Archard JeFoa. Contact and rubbing of flat surfaces. *J Appl Phys* 1953;24(8):981–8.
- [43] Banerjee Sudip, Poria Suswagata, Goutam Sutradhar, Sahoo Prasanta. Dry sliding tribological behavior of AZ31-WC nano-composites. *J Magnes Alloy* 2019;7(2):315–27.
- [44] Wu Liqun, Wu Ruizhi, Hou Legan, Zhang Jinghui, Zhang Milin. Microstructure, mechanical properties and wear performance of AZ31 matrix composites reinforced by graphene nanoplatelets (GNPs). *J Alloys Compd* 2018;750:530–6.
- [45] Wu Liqun, Wu Ruizhi, Hou Legan, Zhang Jinghui, Zhang Milin. Microstructure, mechanical properties and wear performance of AZ31 matrix composites reinforced by graphene nanoplatelets (GNPs). *J Alloys Compd* 2018;750:530–6.
- [46] Chen Wenge, Yang Tao, Dong Longlong, Ahmed Elmasry, Song Jiulong, Deng Nan, Ahmed Elmarakbi, Liu Terence, Lv Hai Bao, Fu Yong Qing. Advances in graphene reinforced metal matrix nanocomposites: mechanisms, processing, modelling, properties and applications. *Nanotechnol Precis Eng* 2020;3(4):189–210.
- [47] Wang Jiajia, Niu Lei, Zhang Yanglin, Chen Jianqing, Jiang Jinghua, Song Dan, Li Baosong, Ying Guobing, Cheng Jiangbo, Ma Aibin. Is Mg17Al12 ductile or brittle? A theoretical insight. *J Magnes Alloys* 2023;11(3):936–44.
- [48] Zhao Rongxia, Zhao Zhanyong, Bai Peikang, Du Wenbo, Di Tie, Zhang Zhen, Wang Liqing, Wang Yu. Research on tribological behavior of graphene with in-situ MgO nanoparticles reinforced AZ91 alloy composite. *CompComm* 2022;30:101086.
- [49] Shahin Mohammad, Munir Khurram, Wen Cuie, Li Yuncang. Nano-tribological behavior of graphene nanoplatelet–reinforced magnesium matrix nanocomposites. *J Magnes Alloy* 2021;9(3):895–909.
- [50] Beniye M, Sivapragash M, Vettivel SC, Senthil Kumar P, Ajith Kumar KK, Niranjan K. Optimization of tribology parameters of AZ91D magnesium alloy in dry sliding condition using response surface methodology and genetic algorithm. *Bull Pol Acad Sci: Tech Sci* 2021;69(1).
- [51] Xiu K, Wang HY, Sui HL, Wang Y, Xu CL, Wang JG, Jiang QC. The sliding wear behavior of TiC p/AZ91 magnesium matrix composites. *J mater Sci* 2006;41:7052–8.
- [52] Aydin Fatih, Sun Yavuz. Investigation of wear behaviour and microstructure of hot-pressed TiB₂ particulate-reinforced magnesium matrix composites. *Can Metall Q* 2018;57(4):455–69.
- [53] Li Pubo, Yang Hua, Gao Mangmang. Microstructure and mechanical properties of multi-scale in-situ Mg₂Si and CNTs hybrid reinforced AZ91D composites. *J Mater Process Technol* 2021;14:2471–85.
- [54] Xiong Bowen, Liu Kang, Yan Qingsong, Xiong Wei, Wu Xiang. Microstructure and mechanical properties of graphene nanoplatelets reinforced Al matrix composites fabricated by spark plasma sintering. *J Alloys Compd* 2020;837:155495.
- [55] Du Xian, Du Wenbo, Wang Zhaohui, Liu Ke, Li Shubo. Ultra-high strengthening efficiency of graphene nanoplatelets reinforced magnesium matrix composites. *Mater Sci Eng A* 2018;711:633–42.
- [56] Li Pubo, Cao Bo, Tan Wanting, Gao Mangmang. Microstructure and synergistic strengthening mechanisms of carbon nanotubes and Mg₂Si nanoparticles hybrid reinforced Mg matrix composites prepared by powder thixoforming. *J Alloy Compd* 2020;818:152925.
- [57] Dieringa Hajo. Properties of magnesium alloys reinforced with nanoparticles and carbon nanotubes: a review. *J Mater Sci* 2011;46:289–306.
- [58] Abdullaev RN, Kozlovskii Yu M, Khairulin RA, Stankus SV. Density and thermal expansion of high purity nickel over the temperature range from 150 K to 2030 K. *Int J Thermophys* 2015;36(4):603–19.
- [59] Sun Xue-fei, Wang Cui-ju, Deng Kun-kun, Kang Jin-wen, Bai Yan, Nie Kai-bo, Shang Shuan-jun. Aging behavior of AZ91 matrix influenced by 5 μm SiCp: investigation on the microstructure and mechanical properties. *J Alloy Compd* 2017;727:1263–72.
- [60] Li Pubo, Tan Wanting, Gao Mangmang, Shi Keren. Strengthening of the magnesium matrix composites hybrid reinforced by chemically oxidized carbon nanotubes and in situ Mg₂Si. *J Alloy Compd* 2021;858:157673.
- [61] Li Pubo, Tan Wanting, Gao Mangmang, Shi Keren. Strengthening of the magnesium matrix composites hybrid reinforced by chemically oxidized carbon nanotubes and in situ Mg₂Si. *J Alloys Compd* 2021;858:157673.
- [62] Wang Pingbo, Shen Jun, Chen Tijun, Li Qinglin, Wang Lingyun. Fabrication of graphene nanoplatelets reinforced Mg matrix composites via powder thixoforming. *J Magnes Alloy* 2022;10(11):3113–32.